Influence of internal electrical losses on optimization of electromagnetic energy harvesting

Shaoyi Zhou, Claire Jean-Mistral, Simon Chesné

Influence of internal electrical losses on optimization of electromagnetic energy harvesting

Shaoyi Zhou, Claire Jean-Mistral and Simon Chesné

Université de Lyon, CNRS INSA-Lyon, LaMCoS UMR5259, F-69621 Villeurbanne, France

E-mail: simon.chesne@insa-lyon.fr

Abstract

A lot of effort has been made to optimize linear electromagnetic energy harvesters under harmonic or random excitation, connected to simple or more complicated electrical extraction circuits. Nevertheless, the internal electrical losses of electromagnetic coils are often neglected in these optimization analyses. To this end, the present paper investigates systematically and for the first time the influence of internal impedance of coils on energy harvesting performance under various types of ambient excitation sources, which are, respectively, external force acting directly on the seismic mass, base displacement-induced motion and disturbance generated by base acceleration. Our analysis highlights that under sinusoidal excitation, the resonant load outperforms its non-resonant counterpart in terms of energy harvesting performance when the internal resistance is very small, while its increase deteriorates significantly the broadband harvesting capability of resonant circuits. When subjected to random vibration, the resonant load presents no advantage compared to the latter one. The optimum design of non-resonant circuit is then carried out in each excitation scenario leading to well-known criteria and expanding to cases where no optimal conditions were defined or obtained. It is also reported that the neglect of internal losses underestimates the maximum available power.

Keywords: vibration energy harvesting, electromagnetic device, shunt circuit optimization

1. Introduction

Energy harvesting from surrounding energy sources has attracted a lot of interest over the past few decades, and becomes a promising technique to supply low consumption of embedded electronic devices, such as actuators and wireless sensors [1–5]. Due to its high availability and ubiquity, mechanical vibration has received considerable attention and numerous transducers have been proposed and extensively studied in the literature, among which three most popular converting principles are: piezoelectric [6], electromagnetic [7] and electrostatic [8].

As initially proposed by Williams and Yates [9], a generic model of energy harvesters can be represented by a mass-spring-damper system of single degree of freedom (SDOF) coupled with an energy transducer. Tremendous research efforts have been devoted to energy harvesting optimization for this SDOF configuration under sinusoidal excitation [9–13], leading to the well-known optimal condition which states that maximum power pumping is observed when the excitation frequency and electrical damping are matched to natural frequency and mechanical damping, respectively. However, as indicated by Tai and Zuo [14], a two-stage process has been adopted by a lot of authors to pursue the maximized energy transfer, in which the excitation and natural frequencies are matched prior to the matching between electrical and mechanical impedances. Nevertheless, in order to maximize the energy extraction from the mechanical to electrical domain, the electrical damping and excitation frequency should be simultaneously involved in the optimization analysis.

For that purpose, Tai and Zuo [14] conducted a two-variable optimization study for a SDOF energy harvester with either electromagnetic or piezoelectric transducer under base-excited harmonic vibration, in which the coil inductance was omitted. The authors revealed that the long-believed optimal condition is correct only in the case of base excitation with constant acceleration amplitude, and is only an approximation for the constant displacement amplitude case under the condition of small mechanical damping (i.e. $< 2\%$). They also underlined that in the latter excitation scenario, the optimal damping ratio and the excitation frequency are always greater than the mechanical damping and the natural frequency, respectively. Despite the novelty in their optimization process, the internal resistance of electromagnetic transducer was considered as a constant ratio of external resistive load instead of a fixed value, and the study was only conducted under specific harmonic cases. Besides, Tang and Zuo [15] investigated the optimization of dual-mass and single-mass electromagnetic energy harvesters under random force and motion excitations with the coil inductance neglected. In [16], the electromagnetic energy harvester is connected with a resonant load and is subject to sinusoidal force excitation. With coil resistance being omitted, it was demonstrated that this specific energy converter exhibits the capability of harvesting maximum power over the whole bandwidth of frequencies. Mann and Sims [17] studied a linear electromagnetic energy harvester connected with a simple resistive load with taking into consideration the total impedance of coil, and it was reported that the influence of coil inductance should not be neglected and its presence could alter the electrical resonance frequency. Wang *et al* [18] investigated the similarity and duality between electromagnetic and piezoelectric energy harvesters by assuming that the internal resistance of coil is negligible. Tang *et al* [19] derived the analytical formulae of electrical parameters for an energy harvester shunted with a resonant circuit under both harmonic and random force excitation, while the coil inductance was neglected. Zhang *et al* [20] investigated the effect of electrical loads containing non-resistive components (i.e. rectifiers and capacitors) on electromagnetic energy harvesting performance. In this work [20], the inductance of coil is again neglected and a conclusion has been drawn that optimum design for a purely resistive load can not be generalized to cases where non-resistive components are involved. However, ignoring a part of internal impedance could result in erroneous remarks for optimization analyses in certain excitation scenarios, which will be addressed in this work. Moreover, these aforementioned works only focused on energy harvesting performance under certain ambient vibration cases, and a complete and uniform optimization encompassing all excitation scenarios has not been yet proposed in literature.

Hence, the motivation and originality of our research is to propose a global optimization study for linear electromagnetic energy harvesting covering four ambient excitation cases and taking into account the internal impedance of electromagnetic transducer. The mechanical structure is shunted with three possible circuits: resistive (*R*), resistive-inductive (*RL*) and resistive-inductive-capacitive (*RLC*). And it undergoes two types of excitations: harmonic and random, which acts directly on the seismic mass (force type), or stems from the base movement (motion type).

The rest of this paper is organized as follows. Section 2 is dedicated to model the energy harvester associated with a generalized *RLC* circuit by taking into account the electrical losses of electromagnetic transducer. In this section, the Laplace transform method is adopted to yield the steady state frequency response. In section 3, the resonant circuit is considered and a three-variable optimization analysis is performed, which underlines the significant influence of electrical losses on its broadband energy harvesting performance. Section 4 considers the non-resonant circuit case, where some original results and optimal formulae of system parameters are presented. In this section, it is reported that the classic optimal condition is not always suitable for all excitation scenarios, and the exclusion of internal losses could result in a considerable underestimation of maximum attainable power, e.g. an underestimate of 10.4% is predicted for an energy harvester with mechanical damping ratio of 0.1 under force harmonic vibration.

2. Electromechanical modeling

We consider an electromagnetic vibration energy harvester, as depicted in figure 1. As mentioned earlier, one can distinguish three possible configurations of harvesting circuitry in practice, which are: (i) *R* type; (ii) *RL* type; (iii) *RLC* type (see figure 2). It is noticeable that the two first circuits can be regarded as particular forms of *RLC* circuit by vanishing certain electrical components. Hence, the proposed generalized model is based on a SDOF energy converter shunted by a resonant *RLC* circuit.

2.1. Force excitation

Figure 1(a) shows a single-mass electromagnetic energy harvester, where an excitation of external forcing type is applied directly on the mass. The equations governing the electromechanical system can de described by

$$M_s\ddot{x} + C_s\dot{x} + K_s x + F_{emf} = F(t) \tag{1a}$$

$$L\dot{i} + Ri + \frac{1}{C}\int i dt - E_{emf} = 0 \tag{1b}$$

where M_s is the seismic mass, C_s denotes the parasitic damping, K_s is the equivalent stiffness, x is the absolute displacement of the seismic mass, i stands for the current induced in the coil, C is the capacitance and a dot denotes differentiation with respect to time. Moreover, $R = R_i + R_e$ and $L = L_i + L_e$ stand for the total resistance and inductance in the circuit, in which the subscripts, i and e, refer to internal impedance of electromagnetic transducer and external electrical loads, respectively.

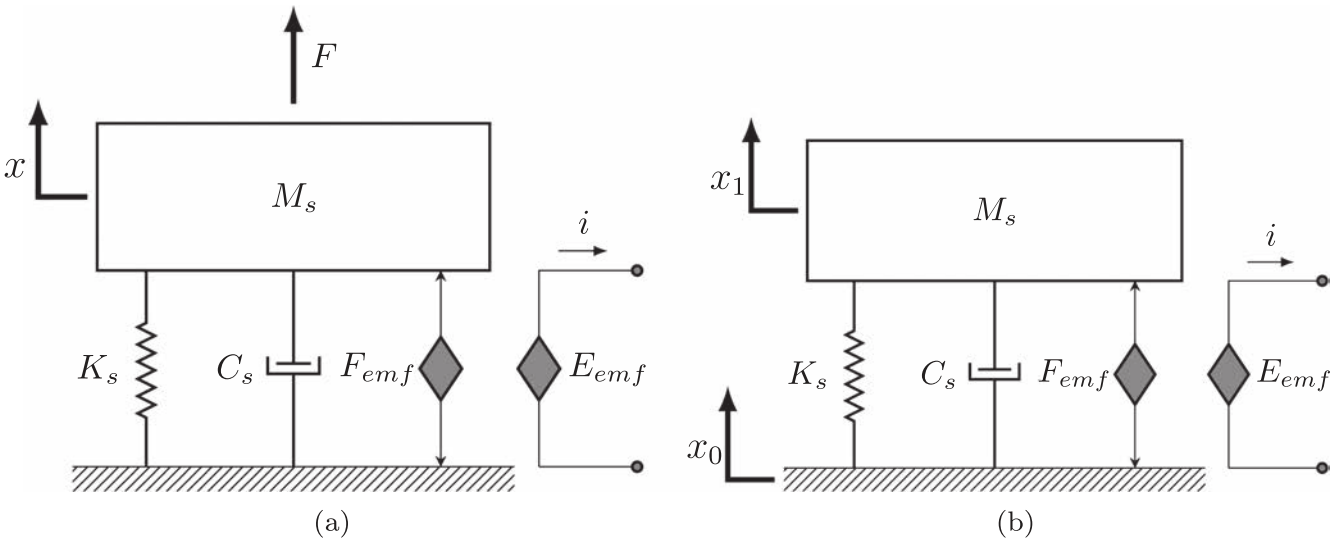

Figure 1. Electromagnetic energy harvester: (a) external force excitation; (b) base excitation.

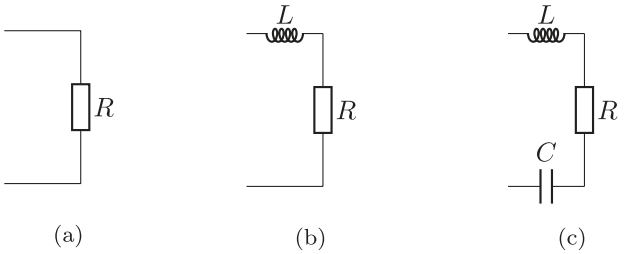

Figure 2. Circuit configurations corresponding to three possible approximations: (a) *R* circuit ($R_i \neq 0$, $L_i = 0$, $C = \infty$); (b) *RL* circuit ($R_i \neq 0$, $L_i \neq 0$, $C = \infty$); (c) *RLC* circuit ($R_i \neq 0$, $L_i \neq 0$, $C \neq \infty$).

$F_{emf} = k_f\, i$ represents the reaction force generated by the electromagnetic transducer and acts on the mechanical subsystem. $E_{emf} = k_v \dot{x}$ indicates the voltage induced in the coil. k_v and k_f are voltage and force constant of electromagnetic transducer, respectively. The relationship between k_v and k_f can be simplified as $k_v = k_f = k_e$.

Taking the Laplace transform of (1) yields to:

$$\frac{I}{F} = \frac{k_e s^2}{(M_s s^2 + C_s s + K_s)(L s^2 + R s + \frac{1}{C}) + k_e^2 s^2} \tag{2}$$

from which the relation between the external force F and square root of power P captured by the external resistive load R_e can be established, and is further written in a dimensionless form as

$$G_f(\bar{s}) = \frac{\sqrt{P}}{F} = \sqrt{R_e}\frac{I}{F} = \frac{k_e\sqrt{R_e}s^2}{(M_s s^2 + C_s s + K_s)(L s^2 + R s + \frac{1}{C}) + k_e^2 s^2}$$
$$= \sqrt{\frac{2}{M_s\omega_s}}\,\frac{\sqrt{\xi_e}\,\kappa\bar{s}^2}{\bar{s}^4 + (2\xi_m + 2\xi_e + \lambda\kappa^2)\bar{s}^3 + (1 + \kappa^2 + \phi^2 + 4\xi_m\xi_e + 2\lambda\xi_m\kappa^2)\bar{s}^2 + (2\xi_e + 2\xi_m\phi^2 + \lambda\kappa^2)\bar{s} + \phi^2}. \tag{3}$$

Where $\bar{s} = s/\omega_s = j\omega/\omega_s = j\alpha$ with $j = \sqrt{-1}$, and these dimensionless parameters are related to the physical properties by

$$\xi_m = \frac{C_s}{2M_s\omega_s},\ \alpha = \frac{\omega}{\omega_s},\ \kappa^2 = \frac{k_e^2}{K_s L}$$
$$\xi_e = \frac{R_e}{2L\omega_s},\ \phi = \frac{\omega_e}{\omega_s},\ \lambda = \frac{M_s\omega_s R_i}{k_e^2}. \tag{4}$$

Where ξ_m is the mechanical damping ratio, ϕ is the frequency tuning ratio, κ^2 is the stiffness ratio (the electromechanical coupling stiffness k_e^2/L divided by the mechanical stiffness K_s), ξ_e is the electrical damping introduced by resistive load R_e, α represents the excitation frequency ω normalized by the natural frequency ω_s, λ indicates the internal electrical loss of coil, $\omega_s = \sqrt{K_s/M_s}$ denotes the undamped natural frequency of mechanical structure and $\omega_e = \sqrt{1/LC}$ refers to the resonant frequency of electrical circuit.

2.2. Motion excitation

The single-mass energy harvester is now subject to motion excitation from the base, as depicted in figure 1(b). And its dynamics in such a scenario can be described by the mathematical model

$$M_s\ddot{x}_1 + C_s(\dot{x}_1 - \dot{x}_0) + K_s(x_1 - x_0) + F_{emf} = 0 \tag{5a}$$

$$L\dot{i} \quad + \quad Ri + \frac{1}{C}\int i dt - E_{emf} = 0 \tag{5b}$$

where x_1 and x_0 are absolute displacement of the seismic mass and moving base, respectively. Under this circumstance, electromagnetic reaction force and induced voltage are defined as: $F_{emf} = k_f\, i$, $E_{emf} = k_v(\dot{x}_1 - \dot{x}_0)$.

Moreover, two types of motion excitations can be distinguished: displacement and acceleration profiles, with the latter one usually employed to model seismic motion.

- Displacement profile:

$$\begin{aligned} G_{x_0}(\bar{s}) &= \frac{\sqrt{P}}{X_0} = \frac{-M_s k_e \sqrt{R_e}\, s^4}{(M_s s^2 + C_s s + K_s)(Ls^2 + Rs + \frac{1}{C}) + k_e^2 s^2} \\ &= -K_s \bar{s}^2 G_f(\bar{s}). \end{aligned} \tag{6}$$

- Acceleration profile:

$$\begin{aligned} G_{\ddot{x}_0}(\bar{s}) &= \frac{\sqrt{P}}{\ddot{X}_0} = \frac{-M_s k_e \sqrt{R_e}\, s^2}{(M_s s^2 + C_s s + K_s)(Ls^2 + Rs + \frac{1}{C}) + k_e^2 s^2} \\ &= -M_s G_f(\bar{s}). \end{aligned} \tag{7}$$

3. Resonant circuit

3.1. Sinusoidal excitation

We firstly carry out the optimum design of a SDOF energy harvester which is shunted with a resonant circuit and is subjected to sinusoidal vibration. By squaring (3), (6) and (7), the normalized harvested power through the resistive load R_e for three excitation scenarios can be expressed as

- Force excitation:

$$\bar{P}_f = \frac{P}{2F^2/M_s\omega_s} = \frac{\xi_e \kappa^2 \alpha^4}{D}. \tag{8}$$

- Displacement excitation:

$$\bar{P}_{x_0} = \frac{P}{2K_s\omega_s X_0^2} = \frac{\xi_e \kappa^2 \alpha^8}{D}. \tag{9}$$

- Acceleration excitation:

$$\bar{P}_{\ddot{x}_0} = \frac{P}{2M_s\ddot{X}_0^2/\omega_s} = \frac{\xi_e \kappa^2 \alpha^4}{D}. \tag{10}$$

It should be mentioned that the normalized power $\bar{P}_f$, $\bar{P}_{x_0}$ and $\bar{P}_{\ddot{x}_0}$ are all dimensionless. And their common denominator D is given by

$$\begin{aligned} D = {} & [AB + (1 + 2\lambda\xi_m)\kappa^2\alpha^2]^2 + 8\xi_m\xi_e\kappa^2\alpha^4 \\ & + 16\lambda\xi_m^2\xi_e\kappa^2\alpha^4 + 16\xi_m^2\xi_e^2\alpha^4 \\ & + (2\xi_e + \lambda\kappa^2)^2\alpha^2A^2 + 4\xi_m^2\alpha^2B^2 - 4\lambda\xi_m\kappa^2\alpha^2AB \end{aligned} \tag{11}$$

with $A = \alpha^2 - 1$ and $B = \phi^2 - \alpha^2$. It is noted from (8) to (10) that the output power is now controlled by electrical damping ratio ξ_e, frequency tuning ratio ϕ and stiffness tuning ratio κ. Mathematically speaking, the global maximum of $\bar{P}(\xi_e, \phi, \kappa)$ is attained at points satisfying the following conditions

$$\frac{\partial\bar{P}}{\partial\phi} = 0, \quad \frac{\partial\bar{P}}{\partial\xi_e} = 0, \quad \frac{\partial\bar{P}}{\partial\kappa} = 0. \tag{12}$$

It is obvious that the harvesting performance is the same under all three excitations and the only difference resides in the change rate of harvested power with respect to excitation frequency α. By solving the previous differential equations (12), two common optimal expressions are found:

$$\phi_{opt} = \alpha\sqrt{1 - \frac{A\kappa^2}{A^2 + 4\xi_m^2\alpha^2}}, \tag{13}$$

$$\xi_{e,opt}^2 = \left(\frac{\xi_m\kappa^2\alpha^2}{A^2 + 4\xi_m^2\alpha^2}\right)^2 + \frac{\lambda^2\kappa^4}{4} + \frac{\lambda\xi_m\alpha^2\kappa^4}{A^2 + 4\xi_m^2\alpha^2}. \tag{14}$$

It is worth noting that the optimal frequency ratio ϕ_{opt} is exactly the same as that in [16], while the optimal electrical damping $\xi_{e,opt}$ deviates from the one in [16], where the difference results from the internal resistive loss λ.

Regarding the stiffness ratio κ, no optimal value could be found. As reported in [16], there is no constraint on the choice of κ at an excitation frequency lower than its natural mechanical frequency ($\alpha \leqslant 1$), while for $\alpha > 1$, the harvested power reaches its maximum if the stiffness remains lower than a maximal value:

$$\kappa \leqslant \kappa_{max} = \sqrt{\frac{A^2 + 4\xi_m^2\alpha^2}{A}}. \tag{15}$$

In this study, the stiffness tuning ratio is chosen as $\kappa_{opt} = 1$ for any $\alpha \leqslant 1$; otherwise, $\kappa_{opt} = \gamma\kappa_{max}$, where γ is a known parameter and is less than unity.

Figure 3 compares electromagnetic energy converters connected with R circuit (i.e. $R_i \neq 0$, $L_i = 0$, $C = \infty$) and RLC circuit (i.e. $R_i \neq 0$, $L_i \neq 0$, $C \neq \infty$), in terms of output power for various internal electrical losses. The metric of harvesting performance is chosen as the half-power bandwidth, which is defined as the frequency bandwidth between which the harvested power is superior to the half of maximum power, as illustrated in figure 3(a). When $\lambda = 0.1$, the half-power bandwidth of RLC circuit is 4.98 times as many as that of resistive load. If the internal loss

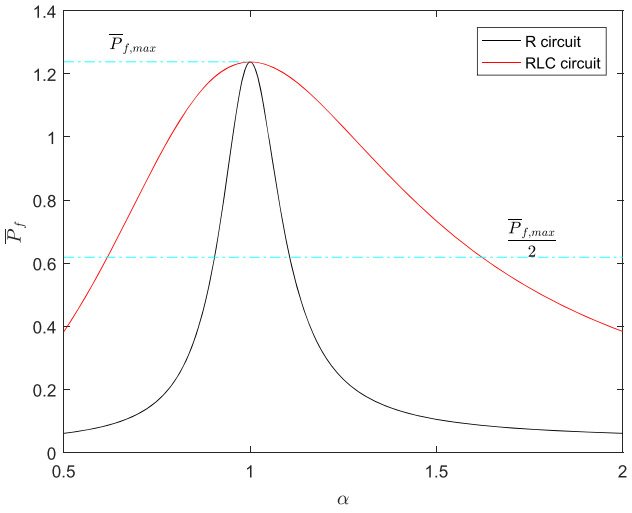

(a) λ = 0.1

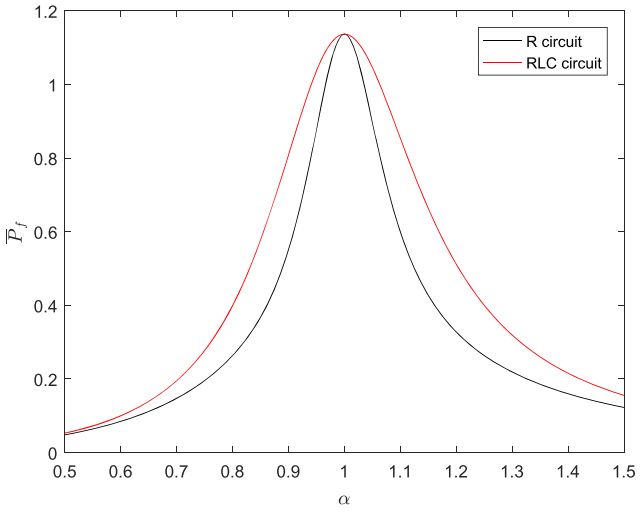

(b) λ = 1

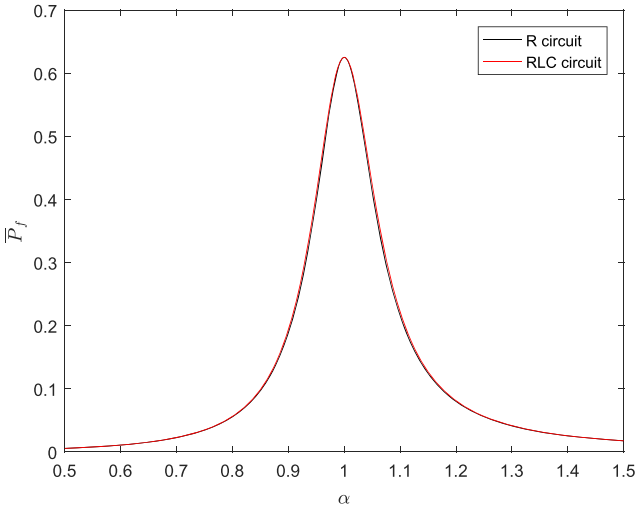

(c) λ = 10

Figure 3. Normalized power $\bar{P}_f$ versus normalized frequency α for $\xi_m = 5\%$ and $\gamma = 0.5$ under harmonic force excitation: (a)–(c) harvesting performance of a SDOF energy scavenger shunted with *R* and *RLC* circuits for different internal electrical losses $\lambda = 0.1$, 1 and 10.

increases to 1, the improvement of resonant load compared to its resistive counterpart is significantly reduced to 63% merely. As λ goes up to 10, the two curves of harvested power relevant to resonant and resistive loads are completely coincident with each other. Therefore, a conclusion can be drawn that compared to simple resistive load, the resonant circuit can harvest energy at higher magnitude over a larger bandwidth when the internal electrical loss λ is relatively small, while this outperformance disappears rapidly as λ increases. One can also remark that the maximum output power is the same for these two electrical extraction circuits (*R* and *RLC*).

Figure 4 summarizes energy harvesting performances of the resonant circuit under different values of internal losses λ. In the case of an idealized transducer (i.e. $\lambda = 0$), the energy scavenger can harvest power at the same magnitude over the whole frequency range, which depends only on the mechanical damping ratio ξ_m and is equal to $1/16\xi_m$ complying with [16]. When a non-idealized transducer is considered, the half-power bandwidth of energy extraction narrows rapidly and the peak output power reduces considerably as the internal electrical loss λ increases. When $\lambda = 0.1$, the dimensionless peak power $\bar{P}_{f,max}$ is 1.238 with its dimensionless half-power bandwidth being 1. As λ arrives at 1, the peak power and half-power bandwidth reduce by, respectively, 8.2% and 67% compared to the case of $\lambda = 0.1$. If a considerable internal loss presents (i.e. $\lambda = 10$), the decreases of peak power and half-power bandwidth become to, respectively, 49.5% and 85.9%.

3.2. Random excitation

3.2.1. Force-induced vibration. The electromagnetic harvester is now subjected to a random force vibration which acts directly on the mass. In light of the stability,

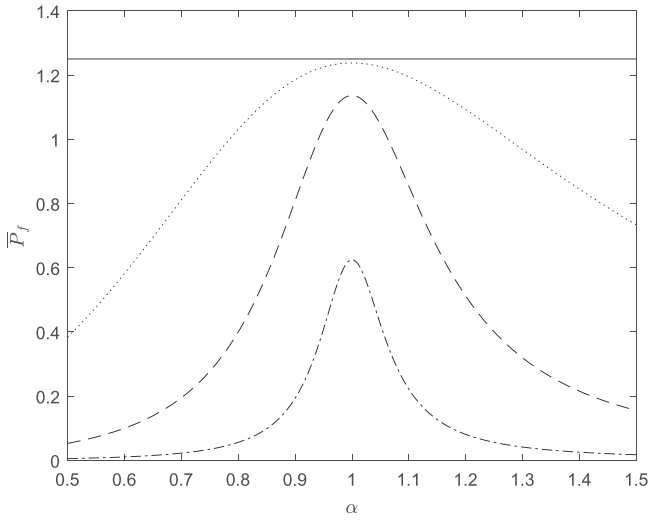

Figure 4. Harvesting performance of a SDOF energy harvester shunted with *RLC* circuit for $\xi_m = 5\%$ and $\gamma = 0.5$ under harmonic force excitation. (—: $\lambda = 0$, ·····: $\lambda = 0.1$, - - -: $\lambda = 1$, -·-·-: $\lambda = 10$).

linearity and time invariance of this energy harvester, the power spectral density (PSD) of harvested power S_p can be formulated as [21]

$$S_p(\bar{s}) = |G_f(\bar{s})|^2 S_i(\bar{s}) \tag{16}$$

where $S_i(\bar{s})$ denotes the PSD of the input random force, considered as a stationary Gaussian process, which has a sufficiently large bandwidth and whose PSD is independent of frequency, i.e. $S_i(\bar{s}) = S_f$.

The mean square value of output power under white noise force excitation of spectral density S_f can be formulated as:

$$E[P_f] = \frac{1}{2\pi}\int_{-\infty}^{\infty} S_p(\bar{s})d\omega = \frac{S_f}{j\pi M_s}\int_{-\infty}^{\infty}\frac{g_4(\bar{s})}{h_4(\bar{s})h_4(-\bar{s})}d\bar{s} \tag{17}$$

where $E[\cdot]$ denotes the mean square value, and these two functions, $g_4(\bar{s})$ and $h_4(\bar{s})$, are defined as

$$\begin{aligned} g_4(\bar{s}) &= b_0\bar{s}^6 + b_1\bar{s}^4 + b_2\bar{s}^2 + b_3 \\ h_4(\bar{s}) &= a_0\bar{s}^4 + a_1\bar{s}^3 + a_2\bar{s}^2 + a_3\bar{s} + a_4 \end{aligned} \tag{18}$$

with all coefficients given by

$$\begin{aligned} &b_0 = 0,\ b_1 = \xi_e\kappa^2,\ b_2 = 0,\ b_3 = 0, \\ &a_0 = 1,\ a_1 = 2\xi_m + 2\xi_e + \lambda\kappa^2,\ a_2 = 1 + 4\xi_m\xi_e + \phi^2 \\ &\quad + (1 + 2\lambda\xi_m)\kappa^2,\ a_3 = 2\xi_e + \lambda\kappa^2 + 2\xi_m\phi^2,\ a_4 = \phi^2. \end{aligned} \tag{19}$$

The indefinite integral in (17) can be calculated by either using the residue theorem [22] or applying directly the analytical formulae provided in [21, 23]. For the sake of completeness, several formulae are annexed in the appendix A. Then, the performance index of harvested power with a resonant circuit is expressed as

$$PI_f = \frac{E[P_f]}{S_f} = \frac{1}{M_s}\frac{a_3 b_1}{a_1 a_2 a_3 - a_0 a_3^2 - a_1^2 a_4}. \tag{20}$$

It is clearly seen from (20) that PI_f is a function of electrical damping ξ_e, frequency tuning ratio ϕ and stiffness ratio κ, i.e. $PI_f = PI_f(\xi_e, \phi, \kappa)$. In order to optimize the energy harvesting performance, a similar approach as in the case of harmonic excitation is employed to locate the global maximum of $PI_f(\xi_e, \phi, \kappa)$, namely:

$$\frac{\partial PI_f}{\partial \xi_e} = 0,\ \frac{\partial PI_f}{\partial \phi} = 0,\ \frac{\partial PI_f}{\partial \kappa} = 0. \tag{21}$$

Now special attention is paid to the optimal condition related to the frequency tuning ratio ϕ, which leads to a polynomial function in ϕ in the concise form of

$$\phi(\phi^2 - 1)(\xi_m\phi^2 + \xi_m + 2\xi_e + \lambda\kappa^2) = 0. \tag{22}$$

Given that ξ_e, ξ_m and λ are all positive, hence only two potential roots can be retained: $\phi_{opt,1} = 0$ and $\phi_{opt,2} = 1$:

(1) $\phi_{opt,1} = 0$. The nullity of $\phi_{opt,1}$ imposes that the electrical resonance does not exist, i.e. $C = \infty$. Therefore, the ultimate energy harvesting performance under random force vibration is attainable by connecting with a non-resonant circuit, which will be investigated in detail in section 4.

(2) $\phi_{opt,2} = 1$. In order to facilitate the optimization analysis, $\phi_{opt,2}$ is substituted in the expression of PI_f. As a consequence, the other two optimal conditions in (21) yield two expressions briefly formulated as:

$$\begin{aligned} &(2\xi_e + 2\xi_m + \lambda\kappa^2)^2 \\ &[(1 + 2\lambda\xi_m)\lambda\kappa^4 + 2(1 + 2\lambda\xi_m)\xi_m\kappa^2 - 8\xi_m\xi_e^2] = 0, \end{aligned} \tag{23a}$$

$$\begin{aligned} &(2\xi_e + 2\xi_m + \lambda\kappa^2)^2 \\ &[(1 + 2\lambda\xi_m)\lambda\kappa^4 - 8\xi_m^2\xi_e - 8\xi_m\xi_e^2] = 0. \end{aligned} \tag{23b}$$

It is noticeable that no rational solutions could be obtained for ξ_e and κ. Therefore, one can reach a conclusion that under random force vibration, no optimal configuration of resonant circuit exists for electromagnetic energy harvesting. In other words, no additional benefits could be obtained by introducing electrical resonance into harvesting circuitry under random vibration.

3.2.2. Base motion vibration. *Base displacement type*. When the energy harvester undergoes a random motion excitation of displacement type, the mean square value of output power is expressed as:

$$\begin{aligned} E[P_{x_0}] &= \frac{\omega_s}{j2\pi}\int_{-\infty}^{\infty}|G_{x_0}(\bar{s})|^2 S_i(\bar{s})d\bar{s} \\ &= \frac{\omega_s S_{x_0}}{j2\pi}\int_{-\infty}^{\infty}|G_{x_0}(\bar{s})|^2 d\bar{s} \end{aligned} \tag{24}$$

where S_{x_0} represents the spectrum of random base displacement, and the integral term can be regarded as the square value of H_2 norm of $G_{x_0}(\bar{s})$. The corresponding

transfer function is defined as

$$G_{x_0}(\bar{s}) = -K_s\sqrt{\frac{2}{M_s\omega_s}}\frac{\sqrt{\xi_e}\kappa\bar{s}^4}{a_0\bar{s}^4 + a_1\bar{s}^3 + a_2\bar{s}^2 + a_3\bar{s} + a_4}. \tag{25}$$

It is remarked that the output power is infinite, which is due to the fact that the rational function $G_{x_0}(\bar{s})$ is not strictly proper, according to Plancherel and Parseval's theorem [24]. Therefore, it suggests that the output power is of ideal white noise type when subjected to random base vibration of displacement profile.

Base acceleration type. Equation (7) implies that when shunted with *RLC* circuit, the optimization procedure of an harvester undergoing a random acceleration disturbance is exactly the same as in the case of random force vibration.

4. Non-resonant circuit

In this section, an optimization analysis of electromagnetic energy harvester connected to a non-resonant circuit ($C = \infty$, $L = L_i$, figure 2(b)) is performed in the scenarios of sinusoidal and random vibration, and some ready-to-use formulae of optimal resistive load are derived analytically.

4.1. Sinusoidal excitation

Given that the frequency tuning ratio $\phi = 0$, the expressions of normalized output power under all three excitation scenarios (8)–(10) can be further simplified into:

- Force- and acceleration-induced excitation:

$$\bar{P}_f = \bar{P}_{\ddot{x}_0} = \frac{\xi_e\kappa^2\alpha^2}{D_1} \tag{26}$$

- Displacement-induced excitation:

$$\bar{P}_{x_0} = \frac{\xi_e\kappa^2\alpha^6}{D_1} \tag{27}$$

where the denominator D_1 can be expressed in a polynomial form of α: $D_1 = \alpha^6 + (c_{11} + c_{12}\xi_e + c_{13}\xi_e^2)\alpha^4 + (c_{21} + c_{22}\xi_e + c_{23}\xi_e^2)\alpha^2 + c_{31} + c_{32}\xi_e + c_{33}\xi_e^2$. The optimal conditions are once again given by:

$$\frac{\partial\bar{P}}{\partial\alpha} = 0, \quad \frac{\partial\bar{P}}{\partial\xi_e} = 0. \tag{28}$$

The solution of optimal electrical damping $\xi_{e,opt}$ is the same for all excitation scenarios (26) and (27), which can be written in the form of polynomial function in α:

$$\alpha^6 + (c_{11} - c_{13}\xi_e^2)\alpha^4 + (c_{21} - c_{23}\xi_e^2)\alpha^2 + c_{31} - c_{33}\xi_e^2 = 0 \tag{29}$$

with all aforementioned coefficients given by:

$$\begin{aligned}
&c_{11} = 4\xi_m^2 + \lambda^2\kappa^4 - 2(1+\kappa^2),\ c_{12} = 4\lambda\kappa^2\ c_{13} = 4,\\
&c_{21} = 1 + 2\kappa^2 + ((1+2\lambda\xi_m)^2 - 2\lambda^2)\kappa^4,\\
&c_{22} = (8\xi_m + 16\lambda\xi_m^2 - 8\lambda)\kappa^2,\ c_{23} = 16\xi_m^2 - 8,\\
&c_{31} = \lambda^2\kappa^4\ c_{32} = 4\lambda\kappa^2,\ c_{33} = 4.
\end{aligned} \tag{30}$$

The optimal expressions of normalized excitation frequency α under different excitation scenarios will be derived separately in the following context.

4.1.1. Force-induced and base acceleration-induced vibration.

In this case, the optimal normalized excitation frequency satisfies the following polynomial law

$$2\alpha^6 + (c_{11} + c_{12}\xi_e + c_{13}\xi_e^2)\alpha^4 - (c_{31} + c_{32}\xi_e + c_{33}\xi_e^2) = 0. \tag{31}$$

In order to solve the simultaneous equations (29) and (31), two different approaches could be imagined. The first approach is described as follows: with (31) being regarded as a cubic equation in α^2, the closed form of optimal α^2 can be then obtained analytically as a function of ξ_e by using the cubic formula provided in [25]; then substituting it into (29), yields an eventual function which depends only on the electrical damping ξ_e, from which one can determine $\xi_{e,opt}$ and consequently α_{opt} can be achieved by the back substitution. The second approach is exactly the reverse sequence of previous one. The authors remark that the latter strategy is more effective to yield optimal expressions in a concise way, which is then adopted in the following study. The optimal expression for α can be eventually given in the form of:

$$(e_1e_4 + e_2e_5)^2 - e_1e_2e_3^2 = 0 \tag{32}$$

where the coefficients are defined as

$$\begin{aligned}
&e_1 = c_{13}\alpha^4 + c_{23}\alpha^2 + c_{33},\ e_2 = \alpha^6 + c_{11}\alpha^4 + c_{21}\alpha^2 + c_{31},\\
&e_3 = c_{32} - c_{12}\alpha^4,\ e_4 = 2\alpha^6 + c_{11}\alpha^4 - c_{31},\ e_5 = c_{13}\alpha^4 - c_{33}.
\end{aligned} \tag{33}$$

One can observe that the polynomial expression (32) is of order 20 in α, the results demonstrated in the following work are then calculated numerically.

Figure 5 depicts the optimization analysis of electromagnetic energy harvesting under harmonic force (or base acceleration) excitation. Two series of simulations have been performed for two extreme cases, namely no electrical losses (—: $\lambda = 0$, $\kappa = 1 \times 10^{50}$) and considerable losses (◦◦◦: $\lambda = 100$, $\kappa = 1$). It is noticeable that as the mechanical damping increases, the optimal α remains unchanged under these extreme circumstances, thus one can conclude that the optimal scenario takes place when an energy harvester is excited at its resonant frequency. Including internal electrical losses in the optimization process leads to the well-known results. Figure 5(b) shows the evolution of optimal normalized resistive load defined as $\bar{R}_e = \xi_e/\kappa^2$ for these two extreme cases. One can notice that $\bar{R}_e$ is dimensionless.

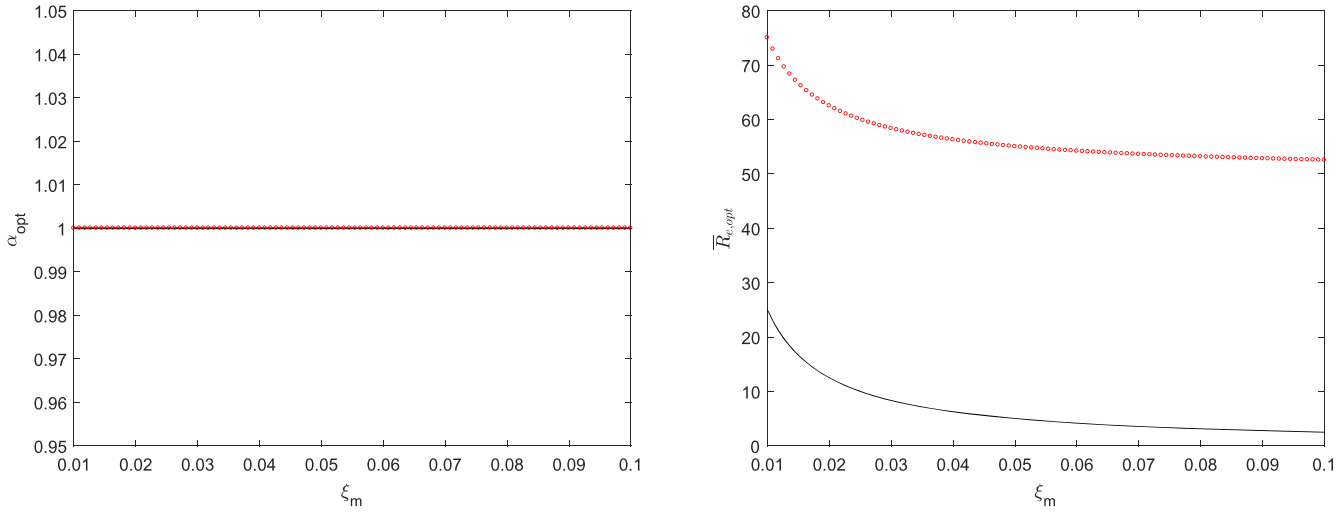

Figure 5. Optimization analysis under harmonic force or base acceleration-induced vibration for two extreme cases (—: $\lambda = 0$, $\kappa = 1 \times 10^{50}$; ◦◦◦: $\lambda = 100$, $\kappa = 1$): (a) optimal normalized excitation frequency α_{opt} against mechanical damping ξ_m; (b) optimal normalized resistive load $\bar{R}_{e,opt}$ versus mechanical damping ξ_m.

Finally, we conclude that the optimal $\bar{R}_e$ is formulated as

$$\bar{R}_{e,opt} = \frac{1}{4\xi_m} + \frac{\lambda}{2} \tag{34}$$

which can be rewritten in a dimensional form as:

$$R_{e,opt} = R_i + \frac{k_e^2}{C_s} \tag{35}$$

which is consistent with the finding of Stephen [11]. As depicted in figures 6(a)–(c), the harvested power including internal losses (34) is always greater than the power harvested without including losses, namely with $\bar{R}_{e,opt} = 1/4\xi_m$. Hence, one can remark that the maximum output power (marked by filled circles in figure 6) can be successfully predicted by using (34) and the exclusion of internal losses will reduce the maximum attainable power. The underestimation of maximum attainable power rises from 0.2% ($\xi_m = 0.01$) to 10.4% ($\xi_m = 0.10$) when internal losses are neglected. In other words, the internal electrical losses can be neglected for lightly damped system, while for moderately or highly damped structure, this simplification can lead to considerable underestimation. And the underestimation of maximum power rises as the mechanical damping ratio ξ_m increases. One can also observe from figure 6 that the normalized power $\bar{P}_f$ and the optimal load $R_{e,\,opt}$ decreases dramatically as the mechanical damping ratio ξ_m increases. Figure 6(d) demonstrates the frequency responses of harvested power in the optimal scenario for three different values of mechanical damping ratio ξ_m. All peaks locate at 1, namely the forcing frequency is equal to the natural frequency and their magnitudes match with the ones found in previous contour plots. And a decrease of 85% is recorded for the maximum achievable power as the mechanical damping ratio ξ_m increases from 0.01 to 0.05.

4.1.2. Displacement-induced vibration. Under this circumstance, the optimal conditions related to α (27) and (28) yield the following expression:

$$(c_{11} + c_{12}\xi_e + c_{13}\xi_e^2)\alpha^4 + 2(c_{21} + c_{22}\xi_e + c_{23}\xi_e^2)\alpha^2 + 3(c_{31} + c_{32}\xi_e + c_{33}\xi_e^2) = 0. \tag{36}$$

Similar to the previous case, the optimal expression with respect to α can be formulated as:

$$(f_1 f_4 + f_2 f_5)^2 - f_1 f_2 f_3^2 = 0 \tag{37}$$

where $f_1 = e_1$ and $f_2 = e_2$, and other coefficients are expressed as:

$$f_3 = -(c_{12}\alpha^4 + 2c_{22}\alpha^2 + 3c_{32}),\ f_4 = c_{11}\alpha^4 + 2c_{21}\alpha^2 + 3c_{31},\ f_5 = c_{13}\alpha^4 + 2c_{23}\alpha^2 + 3c_{33}. \tag{38}$$

The aforementioned strategy is again adopted in this problem. Figure 7 depicts the contours of normalized output power with respect to normalized excitation frequency α and normalized resistive load $\bar{R}_e$ for two cases, namely no electrical losses ($\lambda = 0, \kappa = 1 \times 10^{50}$) and with losses ($\lambda = 5, \kappa = 25$). It is clearly seen from figures 7(a) and (b) that unlike the case of force/base acceleration vibration, the optimal excitation frequency deviates from its resonant frequency and more the mechanical damping increases, more the deviation is important in both cases with and without electrical losses. And it is noted that without electrical losses, no local maximum can be found when the mechanical damping ratio exceeds a certain limit, as shown in figure 7(c). For the purpose of comparison, the maximum powers predicted by the classical formula (34) in the force excitation case and by the exact equation (37) are located for different mechanical damping ratios in figure 7. One can observe that there does exist an extremum of power in the

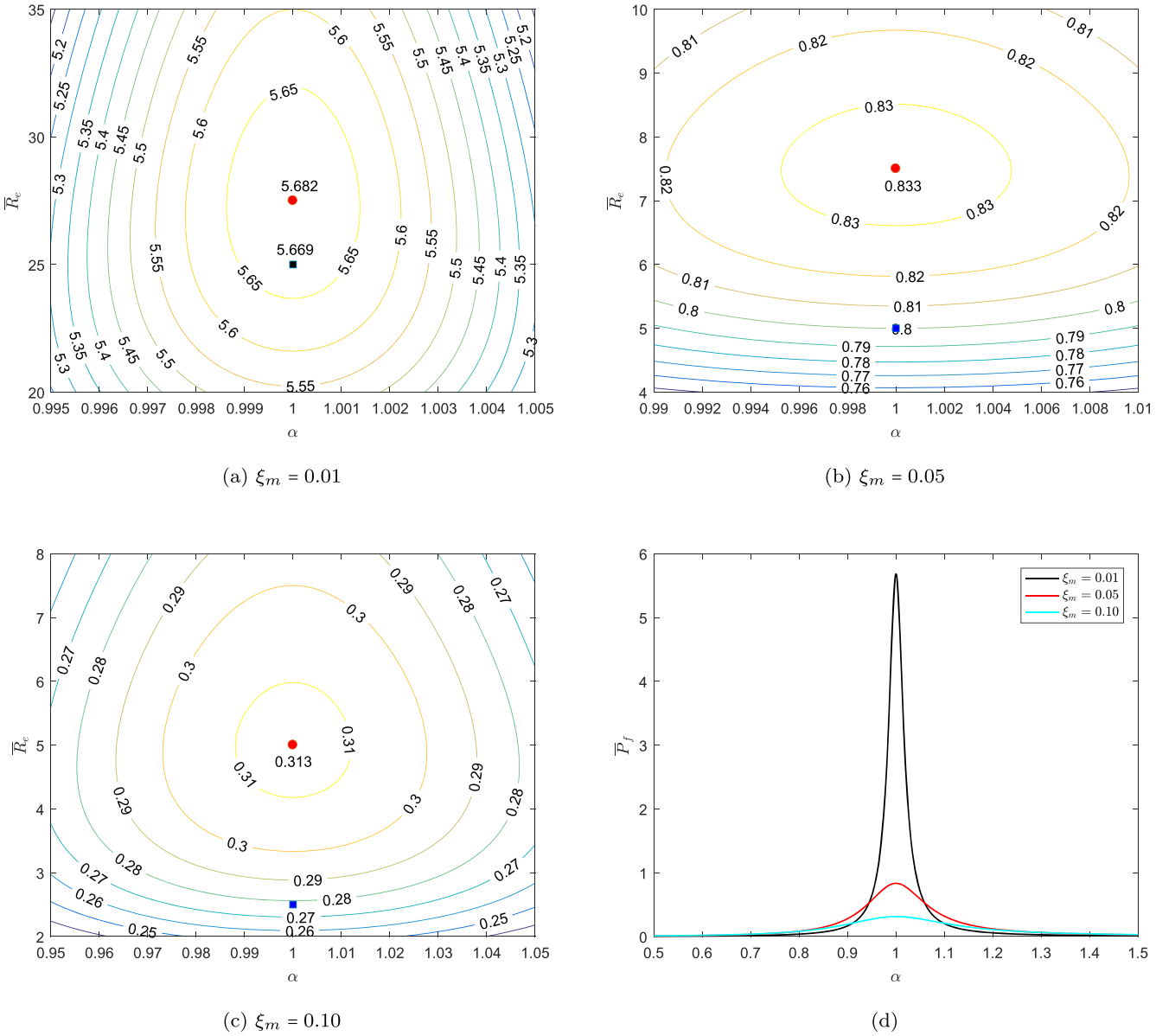

(a) $\xi_m = 0.01$ (b) $\xi_m = 0.05$

(c) $\xi_m = 0.10$ (d)

Figure 6. Harvesting performance under harmonic force or base acceleration-induced vibration for different mechanical damping ratios with $\lambda = 5$ and $\kappa = 25$: (a)–(c) contour of normalized power $\bar{P}_f$(or $\bar{P}_{\ddot{x}_0}$) as a function of α and $\bar{R}_e$ (filled blue square markers: maximum power without electrical losses, filled red circle markers: maximum power predicted by (34) with consideration of internal losses); (d) frequency responses of harvested power with optimal parameter (34) (black line: $\xi_m = 0.01$, red line: $\xi_m = 0.05$, cyan line: $\xi_m = 0.10$).

rational range of mechanical damping ratio ξ_m. It is also noticeable that the maximum power predicted by (34) is close to the exact one when ξ_m is small, while the prediction error becomes considerable as ξ_m increases gradually (at $\xi_m = 0.10$, an underestimate of 7.2% for maximum power is observed and the optimal excitation frequency deviates by 4% from its natural frequency).

Without electrical losses, a critical damping ratio ξ_{cr} has been underlined above which no local maximum can be found. Figure 8 plots the change of critical damping ratio ξ_{cr} as a function of internal resistive loss λ, with excluding the influence of self-inductance of coil, i.e. $\kappa \to \infty$ (the derivation of critical damping is discussed in detail in appendix C). With $\lambda = 0$, the critical damping ratio ξ_{cr} is equal to 0.0754, which agrees with the results in figures 7(a)–(c). Besides, our original optimization analysis highlights that when the resistive loss λ lies in the interval [1, 3.5], the critical damping ratio is always larger than 0.1, which means that there always exist an extremum for a typical mechanical system (i.e. $\xi < 10\%$). If λ resides outside this range, the critical damping ratio ξ_{cr} fluctuates significantly and no evident distribution rule could be distinguished.

4.2. Random excitation

4.2.1. Force-induced vibration. The SDOF electromagnetic energy harvester attached with *RL* circuit, as shown in figure 2(b), is now subject to random force excitation. The frequency tuning ratio ϕ is equal to zero and the generalized

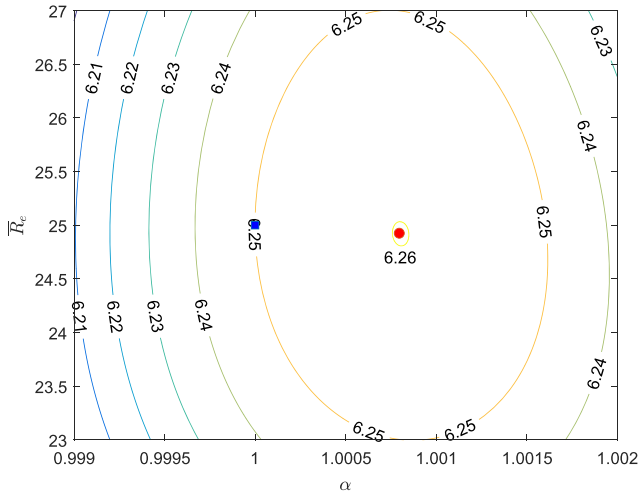

(a) $\xi_m = 0.01$

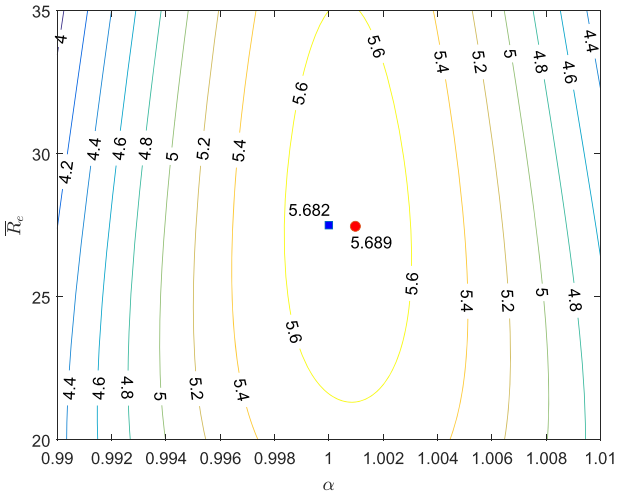

(d) $\xi_m = 0.01$

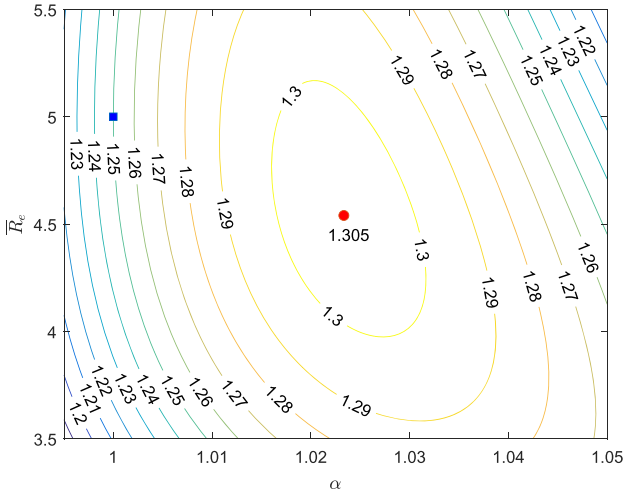

(b) $\xi_m = 0.05$

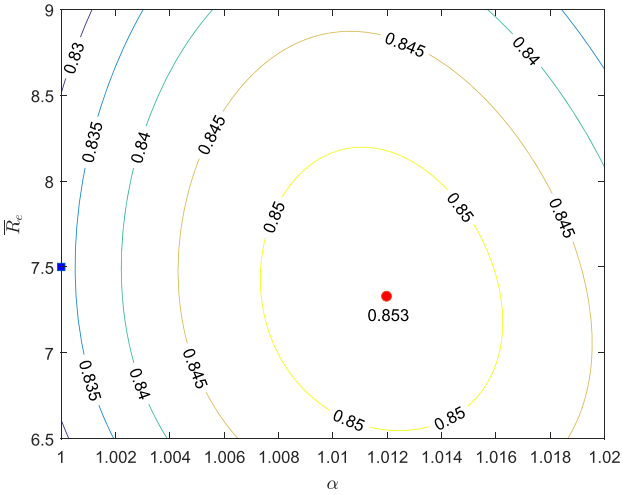

(e) $\xi_m = 0.05$

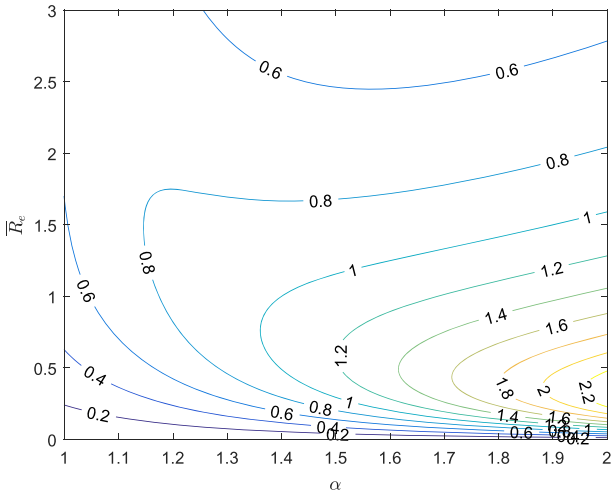

(c) $\xi_m = 0.10$

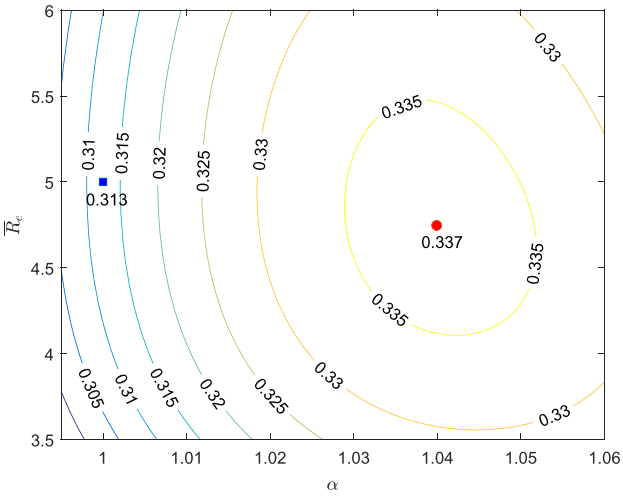

(f) $\xi_m = 0.10$

Figure 7. Contours of normalized output power $\bar{P}_{x_0}$ as a function of α and $\bar{R}_e$ under harmonic base excitation of displacement profile for two series of parameters: (a)–(c) no electrical losses ($\lambda = 0$, $\kappa = 1 \times 10^{50}$); (d)–(f) with electrical losses ($\lambda = 5$, $\kappa = 25$). Filled blue square marker: maximum power predicted by (34) with consideration of internal losses; Filled red circle marker: maximum power obtained by (37).

transfer function (3) can be further reduced to:

$$G_f(\bar{s}) = \sqrt{\frac{2}{M_s\omega_s}}\frac{\sqrt{\xi_e}\kappa\bar{s}}{a_0\bar{s}^3 + a_1\bar{s}^2 + a_2\bar{s} + a_3} \tag{39}$$

with a_0, a_1, a_2 and a_3 defined as previously. Thus, the squared transfer function from the force to the square root of power is simplified as:

$$|G_f(\bar{s})|^2 = \frac{2}{M_s\omega_s} \times \frac{-\xi_e\kappa^2\bar{s}^2}{(a_0\bar{s}^3 + a_1\bar{s}^2 + a_2\bar{s} + a_3)[a_0(-\bar{s})^3 + a_1(-\bar{s})^2 + a_2(-\bar{s}) + a_3]}. \tag{40}$$

It is noticed that a negative sign is present in its numerator, which is due to the fact that $\alpha^2 = -\bar{s}^2$. The mean square value of output power under white noise random force excitation of spectral density S_f can be formulated as:

$$E[P_f] = \frac{1}{2\pi}\int_{-\infty}^{\infty} S_p(\bar{s})d\omega = \frac{S_f}{j\pi M_s}\int_{-\infty}^{\infty}\frac{g_3(\bar{s})}{h_3(\bar{s})h_3(-\bar{s})}d\bar{s} \tag{41}$$

where $E[\cdot]$ denotes the mean square value, and these two functions are defined as, respectively:

$$\begin{aligned} g_3(\bar{s}) &= b_0\bar{s}^4 + b_1\bar{s}^2 + b_2 \\ h_3(\bar{s}) &= a_0\bar{s}^3 + a_1\bar{s}^2 + a_2\bar{s} + a_3 \end{aligned} \tag{42}$$

with $b_0 = 0$, $b_1 = -\xi_e\ \kappa^2$ and $b_2 = 0$. The performance index of energy harvester is then expressed as:

$$PI_f = \frac{E[P_f]}{S_f} = \frac{1}{M_s} \times \frac{\xi_e\kappa^2}{(2\xi_m + 2\xi_e + \lambda\kappa^2)[1 + 4\xi_m\xi_e + (1 + 2\lambda\xi_m)\kappa^2] - (2\xi_e + \lambda\kappa^2)}. \tag{43}$$

From (43), the mean square value of output power $E[P_f]$ is now controlled by the electrical damping ratio ξ_e. The global maximum of $PI(\xi_e)$ is located at points satisfying the following condition:

$$\frac{\partial PI_f}{\partial\xi_e} = 0 \tag{44}$$

which yields the following optimal expression

$$\xi_{e,opt}^2 = \frac{1}{4}\left[1 + (1 + 2\lambda\xi_m)\kappa^2 + (1 + 2\lambda\xi_m)\frac{\lambda\kappa^4}{2\xi_m}\right]. \tag{45}$$

One can also transform (45) into a dimensional form of

$$R_{e,opt}^2 = \omega_s^2 L_i^2 + \frac{k_e^2}{M_s}L_i + \frac{C_s}{M_s}L_iR_i + \frac{k_e^2}{C_s}R_i + R_i^2. \tag{46}$$

The influence of self-inductance can not be excluded if the product $\omega_s\ L_i$ is not ignorable any more. When the self-inductance L_i of coil is negligible, the optimal resistive load is then related to the internal resistance by the following expression

$$R_{e,opt}^2 = R_i^2 + \frac{k_e^2}{C_s}R_i. \tag{47}$$

Substituting the optimal electrical damping ratio (45) into (43), the maximum performance index reads

$$PI_{f,max} = \frac{1}{M_s}\frac{\kappa^2}{2\kappa^2 + 8\lambda\xi_m\kappa^2 + 8\xi_m^2 + 8\xi_m\sqrt{1 + (1 + 2\lambda\xi_m)\kappa^2 + \lambda^2\kappa^4 + \frac{\lambda\kappa^4}{2\xi_m}}}. \tag{48}$$

If the self-inductance L_i is sufficiently small, i.e. $\kappa \to \infty$, the maximum performance index (48) could be further simplified as

$$PI_{f,max} = \frac{1}{M_s}\frac{1}{2 + 8\lambda\xi_m + 4\sqrt{2\lambda\xi_m + 4\lambda^2\xi_m^2}}. \tag{49}$$

Remark 1. The previous expressions indicate that for an electromagnetic energy harvester under random force excitation, there does exist an optimal external electrical load (thus a maximum of output power can be observed), when one considers the presence of internal resistance and self-inductance of coil. This new result contrasts sharply with the conclusion drawn in [15] that no optimal value can be found when internal losses are neglected.

Remark 2. Given that the internal electrical losses R_i and L_i are constant, the optimum energy performance index (48) is a monotonically decreasing function of ξ_m (a detailed derivation is provided in the appendix B). It suggests that a smaller

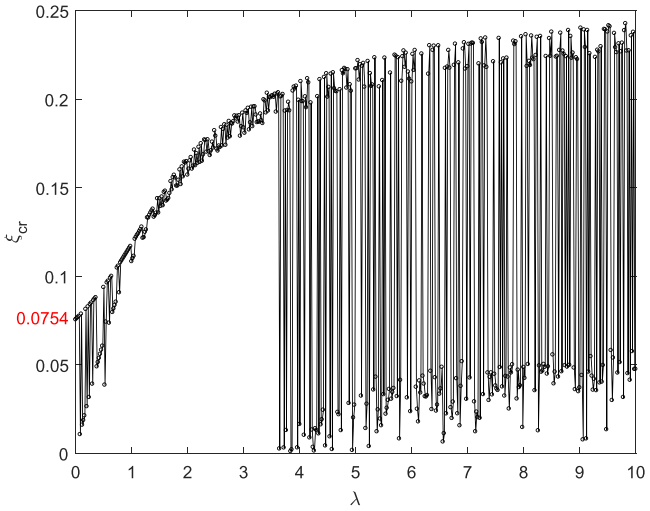

Figure 8. Critical damping ratio ξ_{cr} versus internal resistive loss λ with $\kappa \to \infty$ under harmonic base excitation of displacement profile.

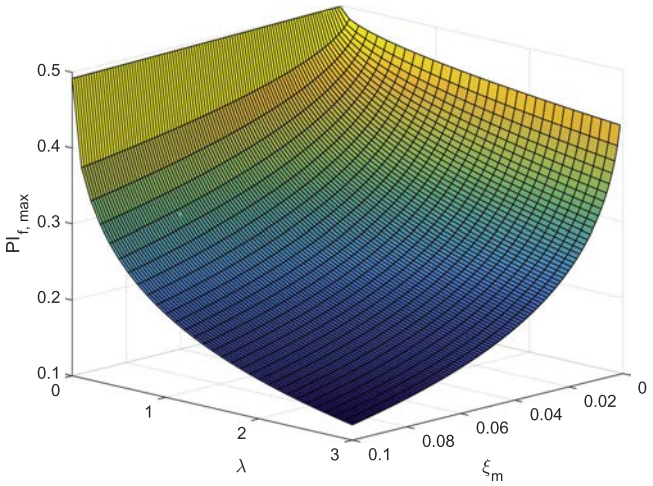

Figure 9. Maximum performance index $PI_{f,max}$ predicted by (48) as a function of mechanical damping ratio ξ_m and internal electrical loss λ under random force excitation with $M_s = 1$ and $\kappa = 25$.

mechanical damping ratio ξ_m is preferred for greater energy harvesting performance, as depicted in figure 9.

Remark 3. As indicated in (48) and (49), the maximum performance index is inversely proportional to the seismic mass M_s. And it is clearly seen from the simplified expression (49) that if the product $\lambda\xi_m$ is constant, a lighter mass will then enhance the harvesting performance under random force excitation.

Remark 4. Considering an extreme case where the electrical losses and inherent mechanical damping are sufficiently small (i.e. $\lambda \to 0$, $\xi_m \to 0$ and $\kappa \to \infty$), then the maximum performance index (48) can be written in an extremely concise form: $PI_{f,max} = 1/2M_s$, which is in accordance with [15]. In this idealized case, the maximum output is only dependent of the seismic mass.

4.2.2. Motion-induced vibration. Base displacement type. When the base displacement is again characterized by a stationary random process, we focus on the corresponding transfer function which leads to:

$$G_{x_0}(\bar{s}) = -K_s\sqrt{\frac{2}{M_s\omega_s}}\frac{\sqrt{\xi_e}\kappa\bar{s}^3}{a_0\bar{s}^3 + a_1\bar{s}^2 + a_2\bar{s} + a_3}. \qquad (50)$$

With this transfer function begin not strictly proper, we conclude that the mean square value of output power in this scenario is infinite, as remarked in section 3.2.2.

Base acceleration type. When the base acceleration is chosen as excitation input, the output power of energy harvester can be related to that under force excitation by $E[P_{\ddot{x}_0}] = M_s^2 E[P_f]$, according to (7). Therefore, the optimization procedure and the optimal formulations are the same as in the circumstance of random force excitation. Besides, the previous remarks 1 and 2 will hold in this scenario, while the last two remarks related to seismic mass (remarks 3 and 4) have to be modified due to the presence of factor M_s^2. Thus the upper bound on the harvested power is reformulated as $E[P]_{\ddot{x}_0,max} = S_{\ddot{x}_0}M_s/2$, which agrees with [26, 27].

5. Conclusions

To the best knowledge of the authors, this paper investigated systematically for the first time the influence of internal electrical losses of electromagnetic transducer on the optimization of electromagnetic energy harvesting under various excitations.

The optimization analysis related to energy harvesting coupled with a *RLC* circuit indicates that, under sinusoidal excitation, the energy converter can exhibit ultra-wide bandwidth harvesting performance in the absence of internal electrical losses, while this capability is considerably influenced by the presence of internal losses. The performance of energy harvester connected with resonant circuits ceases to outperform its counterpart coupled to a simple resistive circuit when the internal loss exceeds a certain threshold. When subjected to random excitation, the authors demonstrate that no additional gain can be attained by introducing electrical resonance in the circuit, i.e. the optimum design under random vibration is to connect electromagnetic transducers with non-resonant circuits.

When shunted by a non-resonant circuit, it is shown that the long-believed optimization condition always holds regardless of magnitude of internal losses under the circumstance of force or base acceleration vibration, while the optimal resistive load should be equal to the sum of internal resistance of coil and the electrical analog of the mechanical damping. In the case of base displacement vibration, the optimal excitation frequency is always greater than the natural frequency, and the degree of deviation depends on the mechanical damping. Besides, there exists a critical damping ratio ξ_{cr}, beyond which no optimum can be achieved. And this threshold is 7.54% in the absence of electrical losses. An evolution of ξ_{cr} with respect to the resistive loss λ is depicted,

which suggests that there always exist a local maximum for a typical mechanical system (i.e. $\xi < 10\%$) if λ satisfies $\lambda \in [1, 3.5]$. When subjected to random excitation, an optimal expression of resistive load is derived analytically in the scenario of force or base acceleration vibration, which contrasts sharply with the existing literature in which the influence of internal losses is excluded and a conclusion has been drawn that no optimum could be obtained. It is also noted that the upper bound of attainable power is only a function of the seismic mass and the PSD of excitation sources.

It should be emphasized that the current work focuses on linear electromagnetic energy harvesting so that the conclusions made and optimal parameters derived can not be extended to cases where nonlinearity presents in the electromechanical system.

Finally, the optimization analyses performed in this paper is based on maximizing the power harvested by the resistive load. Meanwhile, optimum design of harvesters can be also carried out according to other metrics, such as energy harvesting efficiency, which is defined as the ratio between the power harvested by the electrical load and the total input energy. The proposed optimization framework can be easily adapted to analyses according to optimizing the energy harvesting efficiency.

Appendix A. Formulae of indefinite integrals

Several formulae are provided here for indefinite integrals described by

$$I_n = \int_{-\infty}^{\infty} \frac{g_n(x)}{h_n(x)h_n(-x)}dx, \tag{A.1}$$

where n denotes the highest power of $h_n(x)$, with the two functions being in the general form

$$\begin{aligned} g_n(x) &= b_0x^{2n-2} + b_1x^{2n-4} + \cdots + b_{n-1} \\ h_n(x) &= a_0x^n + a_1x^{n-1} + \cdots + a_n. \end{aligned} \tag{A.2}$$

For $n = 3$ and 4, the integrals are analytically formulated by

$$I_3 = j\pi\frac{-a_2b_0 + a_0b_1 - \frac{a_0a_1b_2}{a_3}}{a_0(a_0a_3 - a_1a_2)}, \tag{A.3a}$$

$$I_4 = j\pi \frac{b_0(-a_1a_4 + a_2a_3) - a_0a_3b_1 + a_0a_1b_2 + \frac{a_0b_3}{a_4}(a_0a_3 - a_1a_2)}{a_0(a_0a_3^2 + a_1^2a_4 - a_1a_2a_3)}. \tag{A.3b}$$

Appendix B. Derivative of PI_f with respect to ξ_m

The denominator function of optimum performance index (48) reads

$$D_2 = 2\kappa^2 + 8\lambda\xi_m\kappa^2 + 8\xi_m^2 + 8\xi_m\sqrt{1 + (1 + 2\lambda\xi_m)\kappa^2 + \lambda^2\kappa^4 + \frac{\lambda\kappa^4}{2\xi_m}}. \tag{B.1}$$

Therefore, the derivative of optimum performance index PI_f with respect to mechanical damping ratio ξ_m is formulated as

$$\frac{dPI_f}{d\xi_m} = -\frac{\kappa^2}{M_sD_2^2}\frac{dD_2}{d\xi_m} = -\frac{\kappa^2}{M_sD_2^2}[8\lambda\kappa^2 + 16\xi_m + \frac{8(1 + \kappa^2 + \lambda^2\kappa^4) + 24\lambda\kappa^2\xi_m + \frac{2\lambda\kappa^4}{\xi_m}}{\sqrt{1 + (1 + 2\lambda\xi_m)\kappa^2 + \lambda^2\kappa^4 + \frac{\lambda\kappa^4}{2\xi_m}}}]. \tag{B.2}$$

It is observable that $d\ PI_f/d\ \xi_m < 0$ always holds for any positive value of ξ_m.

Appendix C. Derivation of critical damping ratio ξ_{cr}

By omitting the influence of self-inductance of coil, the eventual optimal expression (37) can be further reduced to a polynomial function in α^2

$$f(\alpha^2) = h_0\alpha^{10} + h_1\alpha^8 + h_2\alpha^6 + h_3\alpha^4 + h_4\alpha^2 + h_5 = 0 \tag{C.1}$$

with all coefficients defined as

$$h_0 = -8\ \lambda^2, \tag{C.2a}$$

$$h_1 = -80\ \lambda^2\xi_m{}^2 + 56\ \lambda^2 - 40\ \lambda\ \xi_m - 9, \tag{C.2b}$$

$$h_2 = -128\ \lambda^2\xi_m{}^4 + 304\ \lambda^2\xi_m{}^2 - 128\ \lambda\ \xi_m{}^3 - 144\ \lambda^2 + 152\ \lambda\ \xi_m - 32\ \xi_m{}^2 + 39, \tag{C.2c}$$

$$h_3 = 384\ \lambda^2\xi_m{}^4 - 432\ \lambda^2\xi_m{}^2 + 384\ \lambda\ \xi_m{}^3 + 176\ \lambda^2 - 216\ \lambda\ \xi_m + 96\ \xi_m{}^2 - 55, \tag{C.2d}$$

$$h_4 = 208\ \lambda^2\xi_m{}^2 - 104\ \lambda^2 + 104\ \lambda\ \xi_m + 25, \tag{C.2e}$$

$$h_5 = 24\ \lambda^2. \tag{C.2f}$$

As mentioned in [14], the necessary and sufficient condition of absence of local maximum for a polynomial equation is that its corresponding discriminate is equal to zero. Given that (C.1) is of order 5 in α^2, the critical damping ξ_{cr} at each value of λ is estimated numerically by using Maple. For $\lambda = 0$, the previous quintic equation (C.1) is reduced to cubic one, and its discriminate can be analytically expressed as

$$\begin{aligned} \triangle_3 &= h_1^2h_2^2 - 4h_0h_2^2 - 4h_1{}^3h_3 - 27h_0^2h_3^2 + 18h_0h_1h_2h_3 \\ &= 4096\xi_m^2(2304\xi_m^6 + 320\xi_m^4 - 2639\xi_m^2 + 15) = 0 \end{aligned} \tag{C.3}$$

which yields the value at $\xi_{cr,\lambda=0} = 0.0754$, validating the finding in [14].

ORCID iDs

Shaoyi Zhou https://orcid.org/0000-0002-1739-5729

References

[1] Roundy S and Wright P K 2004 A piezoelectric vibration based generator for wireless electronics *Smart Mater. Struct.* **13** 1131–42

[2] Anton S R and Sodano H A 2007 A review of power harvesting using piezoelectric materials (2003–2006) *Smart Mater. Struct.* **16** R1–21

[3] Harne R L and Wang K W 2013 A review of the recent research on vibration energy harvesting via bistable systems *Smart Mater. Struct.* **22** 023001

[4] Roundy S 2005 On the effectiveness of vibration-based energy harvesting *J. Intell. Mater. Syst. Struct.* **16** 809–23

[5] Lee S *et al* 2009 Robust segment-type energy harvester and its application to a wireless sensor *Smart Mater. Struct.* **18** 095021

[6] Erturk A and Inman D J 2008 Issues in mathematical modeling of piezoelectric energy harvesters *Smart Mater. Struct.* **17** 065016

[7] Wang L and Yuan F G 2008 Vibration energy harvesting by magnetostrictive material *Smart Mater. Struct.* **17** 045009

[8] Boisseau S, Despesse G and Sylvestre A 2010 Optimization of an electret-based energy harvester *Smart Mater. Struct.* **19** 075015

[9] Williams C B and Yates R B 1996 Analysis of a micro-electric generator for microsystems *Sensors Actuators* A **52** 8–11

[10] Roundy S, Wright P K and Rabaey J 2003 A study of low level vibrations as a power source for wireless sensor nodes *Comput. Commun.* **26** 1131–44

[11] Stephen N G 2006 On energy harvesting from ambient vibration *J. Sound Vib.* **293** 409–25

[12] Saha C R, O'Donnell T, Loder H, Beeby S and Tudor J 2006 Optimization of an electromagnetic energy harvesting device *IEEE Trans. Magn.* **42** 3509–11

[13] DuToit N E, Wardle B L and Kim S 2005 Design considerations for mems-scale piezoelectric mechanical vibration energy harvesters *Integr. Ferroelectr.* **71** 121–60

[14] Tai W and Zuo L 2017 On optimization of energy harvesting from base-excited vibration *J. Sound Vib.* **411** 47–59

[15] Tang X and Zuo L 2012 Vibration energy harvesting from random force and motion excitations *Smart Mater. Struct.* **21** 075025

[16] Caruso G 2015 Broadband energy harvesting from vibrations using magnetic transduction *Trans. ASME. J. Vib. Acoust.* **137** 2431138

[17] Mann B P and Sims N D 2010 On the performance and resonant frequency of electromagnetic induction energy harvesters *J. Sound Vib.* **329** 1348–61

[18] Wang X, John S, Watkins S, Yu X, Xiao H, Liang X and Wei H 2015 Similarity and duality of electromagnetic and piezoelectric vibration energy harvesters *Mech. Syst. Signal Process.* **52–53** 672–84

[19] Tang X, Liu Y, Cui W and Zuo L 2016 Analytical solutions to h_2 and h_∞optimizations of resonant shunted electromagnetic tuned mass damper and vibration energy harvester *Trans. ASME. J. Vib. Acoust.* **138** 011018

[20] Zhang H, Corr L R and Ma T 2018 Effects of electrical loads containing non-resistive components on electromagnetic vibration energy harvester performance *Mech. Syst. Signal Process.* **101** 55–66

[21] James H M, Nichols N B and Phillips R S 1947 *Theory of servomechanisms* (New York: M.I.T. Radiat. Lab., McGraw-Hill)

[22] Bak J and Newman D J 2010 *Applications of the Residue Theorem to the Evaluation of Integrals and Sums* (New York: Springer) pp 143–60

[23] Jeffrey A, Zwillinger D, Gradshteyn I S and Ryzhik I M (ed) 2007 3–4—definite integrals of elementary functions *Table of Integrals, Series, and Products* 7th edn (Boston: Academic) pp 247–617

[24] de Oliveira M C 2017 *Fundamentals of Linear Control: A Concise Approach* (Cambridge: Cambridge University Press)

[25] Weisstein E W 2002 Cubic formula *Omega* **86** 87

[26] Halvorsen E 2008 Energy harvesters driven by broadband random vibrations *J. Microelectromech. Syst.* **17** 1061–71

[27] Langley R S 2014 A general mass law for broadband energy harvesting *J. Sound Vib.* **333** 927–36